Bull Eng Geol Env (2007) 66: 71–79
DOI 10.1007/s10064-006-0056-z

ORIGINAL PAPER

Murat Karakus
Aydın Ozsan
Hakan Başarır

Finite element analysis for the twin metro tunnel constructed in Ankara Clay, Turkey

Received: 22 December 2005
Accepted: 28 April 2006
Published online: 7 July 2006
© Springer-Verlag 2006

M. Karakus (✉) · H. Başarır
School of Engineering, Inonu University,
44280 Malatya, Turkey
E-mail: mkarakus@inonu.edu.tr
Tel.: +90-422-3410030
Fax: +90-422-3410046

A. Ozsan
Department of Geological Engineering,
Ankara University, 06100 Ankara, Turkey

Abstract The paper presents the geotechnical properties along the route of the 9,325 m twin tunnel metro route in the Greater Municipality of Ankara. Convergence measurements taken during tunnel construction are presented and discussed. In addition, the convergence of the twin metro tunnels was analysed by means of a 2D plane strain finite element (FE) analysis. The FE model estimations and the field measurements are compared.

Keywords Twin metro tunnel · Finite element · Tunnel convergence · Ankara Clay

Résumé L'article présente les propriétés géotechniques des terrains le long du tracé du tunnel bi-tubes du métro à Ankara. Les mesures de convergence réalisées durant la construction des tunnels sont présentées et discutées. De plus, cette convergence a été modélisée à partir d'une méthode aux éléments finis, à deux dimensions, en déformation plane. Les résultats de la modélisation et les mesures de terrain ont été comparées.

Mots clés Tunnel · Convergence · Ankara · Turquie

Introduction

Tunnelling in urban areas is increasing and often requires excavation of a new tunnel to join an existing or newly constructed one. Constructing multiple tunnels, e.g. excavation of twin metro tunnels side-by-side or piggybacked, presents greater engineering challenges. As well as the geological settings along the tunnel route and stand up times, ground movements due to the excavation of an adjacent tunnel also need to be understood and the interactions between the two excavations assessed. In this paper the geological and geotechnical properties along the MTA tunnel route and the monitoring of tunnel closure are presented. The results of a finite element model (FEM) developed to investigate ground movements into the tunnel have been compared with the measured convergence values.

The location of the twin metro tunnel is illustrated in Fig. 1. Each tunnel is approximately 7 m in diameter with the distance between the centrelines being kept within 15 m. The twin tunnels were driven at shallow depth, mainly through Ankara Clay, which oedometer test results indicated to be lightly overconsolidated. Thus the Modified Cam Clay model, which was developed to represent normally or lightly overconsolidated soil behaviour, was used in the finite element (FE) analysis. The made ground over the Ankara Clay was modelled using the Drucker–Prager plasticity model in which the failure function is dependent on the intermediate principal stress. In order to achieve deformations and the 3D tunnelling effect in 2D FE analysis, the hypothetical modulus of elasticity (HME) soft lining approach was adopted.

Excavation of the tunnel was carried out in two stages. Firstly, the upper heading was excavated and immediately shotcreted with a 30 mm thick cover, after which steel mesh and lattice girders were emplaced and a further 170 mm of shotcrete was applied. The lower part

Fig. 1 Location of the tunnels

of the tunnel was excavated and the support elements were installed in the same manner. In order to provide stability, the pull of the excavation was kept within 1–1.5 m in each advance and the lower part of the excavation followed a maximum of 6 m behind the excavation of the upper heading. Thus the support ring was closed as early as possible in order to avoid excessive displacements.

Numerical methods are widely used to analyse ground support interactions, deformations and stress redistributions around an underground opening (Ozsan and Basarir 2003; Ozsan and Karpuz 2001; Kontogianni and Stiros 2002). Most potential hazards associated with excavations can be calculated using these methods.

The convergence of a tunnel (the amount of closure relative to the tunnel diameter) is a significant indication of the deformation. In order to maintain stability, the amount of closure should be precisely measured and the necessary support measures determined (Kovari and Amstad 1993). Short-term convergence measurements on 31-03-2003 and 10-04-2003 indicated the maximum displacement was at the crown of the right tunnel.

Geology and geotechnical properties of the construction site

The soil profile for the tunnel route consists of made ground and Ankara Clay (Fig. 2). The fill was brown in colour, and composed of uncompacted blocky gravel with rubble and sandy clay. The thickness ranged from 0.8 to 7.5 m.

The Ankara Clay was brown to reddish-brown in colour and composed of mainly silty, sandy clay with clayey silt. Ordemir et al. (1965) describe the Ankara Clay as fine reddish-brown clastics with a high proportion of clay while Erol (1973) found that locally there were very thin calcareous horizons, nodules and concretions at shallow depth within the clayey levels which vary in thickness. As the Ankara Clay has a low permeability, there is no clear water level. X-ray analyses show the Ankara Clay consists of the smectite group of clay minerals, illite and montmorillonite (Ordemir et al. 1977; Erguler and Ulusay 2003). According to the Unified Soil Classification System, it comprises high plasticity (CH), highly compressible inorganic silt and organic clays (MH). The fissured clay has a swelling potential due to the montmorillonite and illite contents.

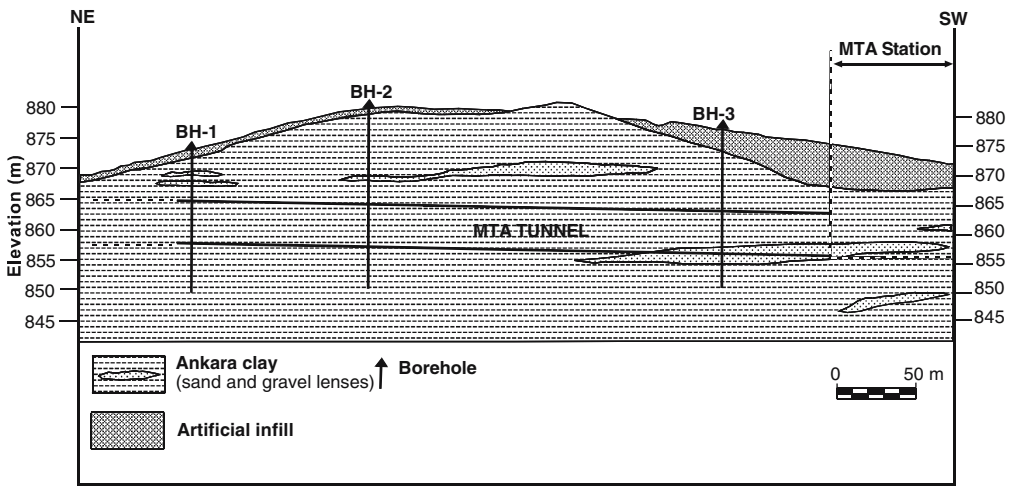

Fig. 2 Geological profiles along the MTA tunnel route

Table 1 Standard penetration test results for Ankara Clay

Depth, m	Very soft $N=(0–1)$	Soft $N=(2–4)$	Firm $N=(5–8)$	Stiff $N=(9–15)$	Very stiff $N=(16–30)$	Hard $N>30$
0–10	–	–	–	6	38	56
10–20	–	–	–	–	–	100
20–30	–	–	–	–	–	100
>30	–	–	–	–	–	100

N number of blows

Table 2 Soil properties of the Ankara Clay

Parameters, symbols, unit	Values
Moisture content, w, %	32
Liquid limit, LL, %	73
Plastic Limit, PL, %	37
Plasticity Index, PI	36
Unified Soil Classification System	MH, ML, CH
Void ratio, e	0.94

The results of the Standard Penetration Tests are given in Table 1 and the results of the laboratory tests carried out on undisturbed soil samples taken from the MTA tunnel route are given in Table 2.

The stress–strain relationship was determined using the Modified Cam Clay model. The Modified Cam Clay yield function is defined in terms of the equivalent effective pressure stress (p') and the deviator stress (q') which are relevant to the interpretation of soil response in the conventional triaxial test (Roscoe and Burland 1968).

Parameters to locate the compression and swelling lines and specific volume at $\ln p' = 1.0$ in Fig. 3 have been defined in the isotropic consolidation section. The equation for the yield locus in the original Cam Clay model is given as:

$$q = Mp' \ln\left(\frac{p'_o}{p'}\right) \tag{1}$$

where p'_o is the isotropic pre-consolidation pressure and M is a material constant defined in terms of the angle of friction (Table 3). The shape of the yield locus is a bullet shape while the Modified Cam Clay yield locus is an elliptical shape. Then the equation becomes as follows:

$$f = M^2 p'^2 - M^2 p'_o p' + q^2 = 0 \tag{2}$$

If the soil obeys the normality condition, i.e. the yield surfaces and plastic potential surfaces are identical, then the yield locus and plastic potential in the $p' : q$ plane are given by the formula above. The recoverable strain or elastic region is assumed inside the yield locus. Beyond the ellipse—in the plastic region—irrecoverable strain occurs.

The made ground above the Ankara Clay has been modelled using the Drucker–Prager perfectly plastic model. The failure function is dependent on the value of

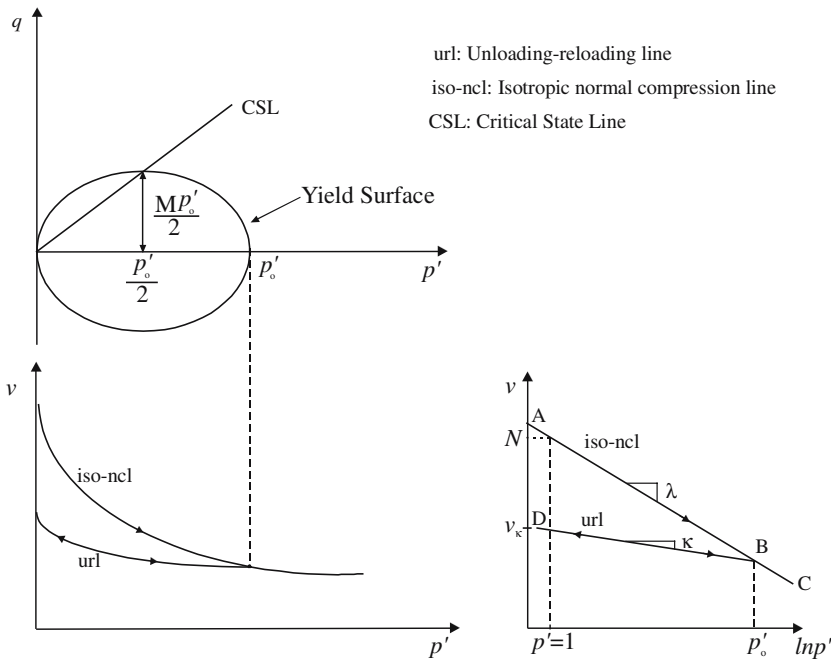

Fig. 3 Elliptical yield locus, isotropic compression line and compression and swelling line in p':q:e plane for the Modified Cam Clay model (after Wood 1990)

Table 3 Soil properties adopted in the FE analysis

Parameter, unit and symbols	Undrained properties Ankara Clay	Drained properties Made ground
Unit weight, kN/m^3, γ	20	20
Poisson's ratio, ν	0.2	0.2
Log. elastic bulk modulus, κ	0.025	N/A
Log. plastic bulk modulus, λ	0.065	N/A
Bulk modulus of water, MN/m^2, K_w	2,200	N/A
Initial void ratio, e_0	1.04	–
Stress ratio at critical state $M = 6\sin\phi/(3-\sin\phi)$	0.9	N/A
Friction angle, φ, degree	23°	35°
Cohesion, c, kPa	–	10
Young's modulus, MPa, E'	–	50

N/A not applicable

the intermediate principal stress. Typical geotechnical materials generally include some small dependence on the intermediate principal stress. Thus, the Drucker–Prager yield model can be more accurate for soil and rock applications. The yield function is given by:

$$f = \alpha J_1 + \sqrt{J_2} = k \tag{3}$$

where α and k are the material constants that can be related to Mohr–Coulomb's material constants c (cohesion) and φ (internal friction angle). The relationships then become:

$$\alpha = \frac{2\sin\phi}{\sqrt{3}(3-\sin\phi)} \tag{4}$$

$$k = \frac{6c\cos\phi}{\sqrt{3}(3-\sin\phi)}. \tag{5}$$

The parameter J_1 is the first invariant of the stress tensor, i.e. the sum of the principal stresses and J_2 is the second invariant of the deviatoric stress tensor given by:

$$J_2 = \frac{1}{6}\left[(\sigma_1-\sigma_2)^2 + (\sigma_2-\sigma_3)^2 + (\sigma_3-\sigma_1)^2\right] \tag{6}$$

The yield or failure surface for Eq. 3 in principal stress space is a right-circular cone with the symmetry about the hydrostatic axis. The plastic deformation is accompanied by an increase in volume.

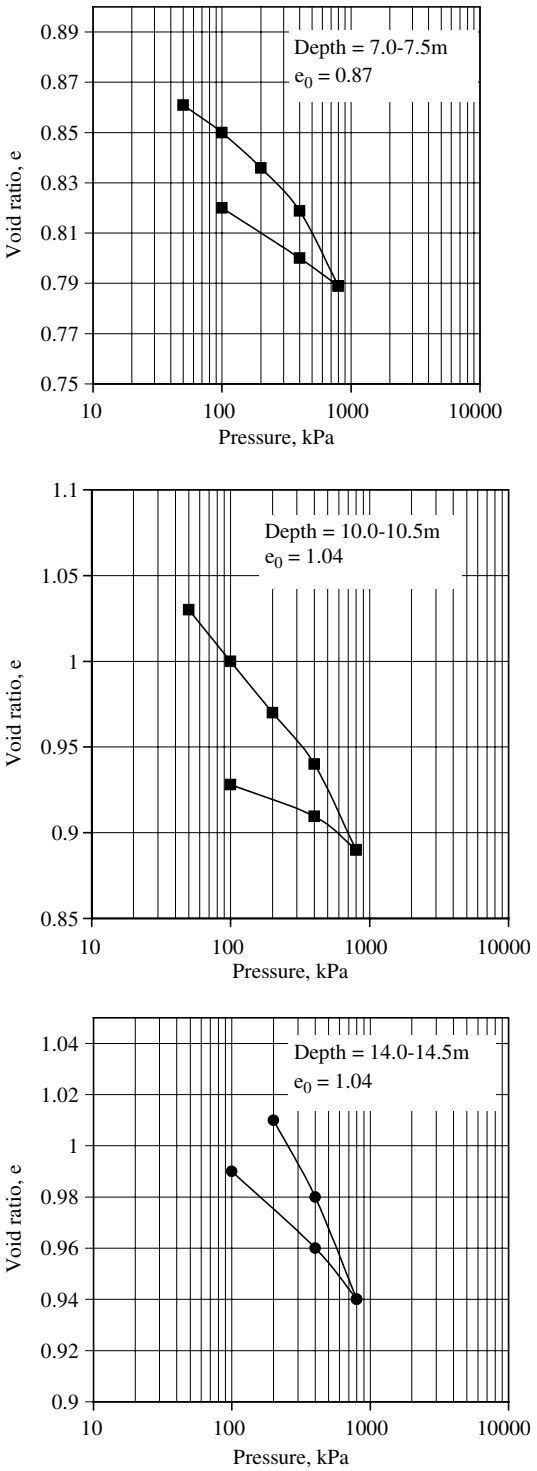

Fig. 4 Some of the consolidation test results shown for illustrative purposes

Finite element analysis

The Modified Cam Clay parameters adopted in the FE analysis were based on the oedometer test results, some of which are given in Fig. 4. The parameters are presented in Table 3. In order to carry out undrained analysis for the Ankara Clay the bulk modulus of water (K_w), was calculated using the following expression:

$$K' = \frac{(1+e) \times p'}{\kappa} \quad (7)$$

where K' is the effective bulk modulus of water, p' is the effective mean normal stress, e is void ratio and κ is the logarithmic elastic bulk modulus. In an undrained analysis, K_w is normally taken as $100 \times K'$.

Finite element analysis was carried out with the 90 m×53.5 m deep mesh (Fig. 5). The detailed tunnel geometry and the structural elements are given in Fig. 6. The model was fixed in the horizontal directions on both left and right sides and the bottom part of the mesh was pinned. Non-consolidating eight-noded linear strain quadrilaterals and non-consolidating six-noded linear strain triangular elements were used for the soil medium. Shotcrete and concrete were modelled using LSQ elements.

As the tunnel excavation was performed in two stages in the field, the same construction method was employed in the FE analysis. Details of the excavation sequences are illustrated in Fig. 7. After achieving equilibrium at the initial stage, the upper heading of the left tunnel was excavated and solid continuum elements representing shotcrete were activated with the predetermined HME value (Karakus and Fowell 2003, 2005). This was provided to account for deformations due to volume loss, a percentage of the theoretical tunnel volume.

The shotcrete thickness assigned was 200 mm and the selected short-term modulus of elasticity of shotcrete was taken as 8 GPa. The concrete applied over the shotcrete was assigned a 400 mm thickness and an elasticity modulus of 20 GPa.

Each tunnel excavation and construction was carried out in five steps. Increments for each step were kept within 20 increments, which was found to be sufficient to reach equilibrium. Support elements have been introduced in a single increment. It was seen that running analyses in a small number of increments led to divergence of forces within the soil body when modelling the excavation.

Evaluation of the results

Convergence measurements were carried out after the shotcrete was applied to the tunnel periphery before the permanent 400 mm concrete wall was installed. Topographical measurement techniques were utilised to monitor the actual convergence of the tunnel. The convergence measurements points are shown in Fig. 6. It was appreciated that some measurements may be erroneous as convergence pins attached to the tunnel walls suffered some damage due to the working equipment in the tunnel. In addition, water locally trapped in the clay caused swelling which led to changes in the pin locations from time to time. Table 4 shows the observed and the calculated convergence values. The field measurements given in the table correspond to the upper and lower parts of the left tunnel excavation and the upper, left lower and the upper part of the right tunnel excavation.

Vertical displacements corresponding to the left tunnel upper excavation, the left tunnel lower excavation and the right tunnel upper excavation are in agreement with the field observations. However, the horizontal

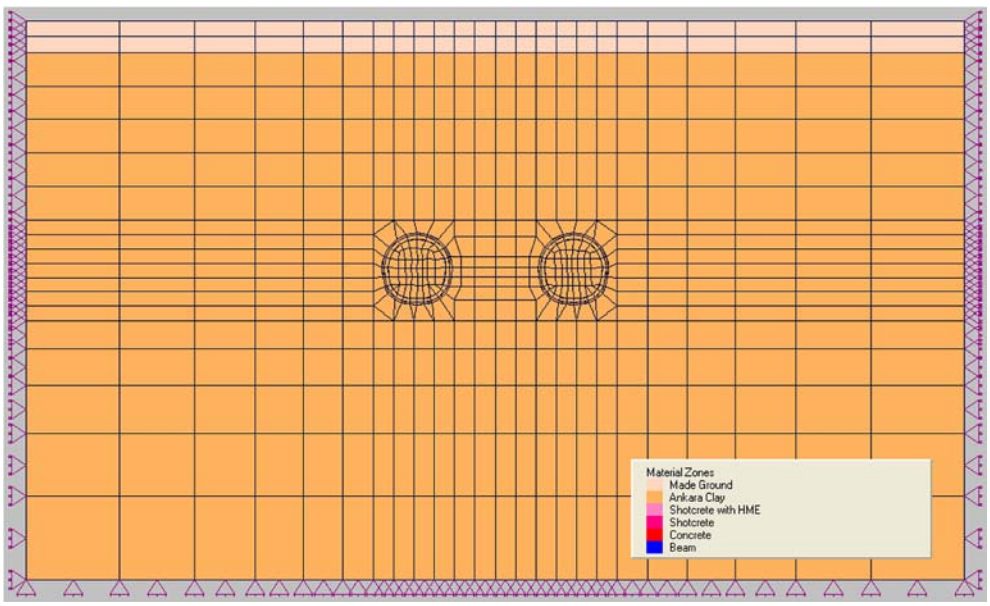

Fig. 5 Finite element mesh used in the analysis

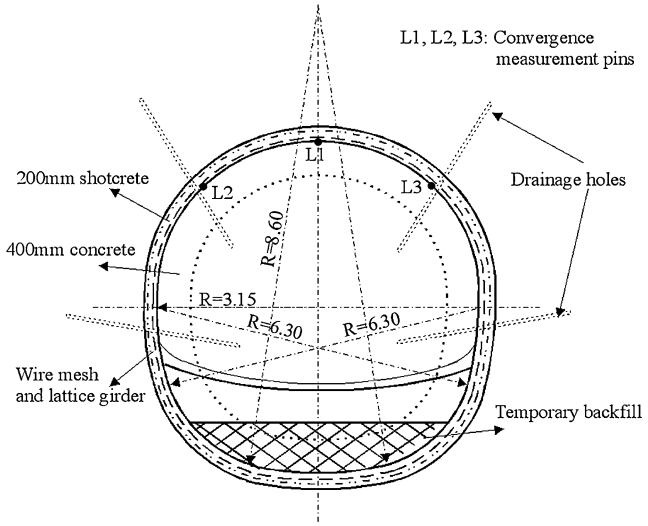

Fig. 6 Constructed tunnel geometry (not to scale)

displacements on the tunnel walls deviated from the field measurements. For the left tunnel lower excavation, however, the FEM calculations correctly predicted zero displacements; the selected shotcrete thickness being sufficient to stop excessive convergences.

Figures 8, 9, 10 and 11 shows the 10-day differential convergence observations for both left and right tunnels. No real time FEM simulation was carried out, but the displacement predictions obtained are provided in Table 4. As can be seen from Fig. 8, horizontal displacement at station L2 seem to stop around 4 mm displacement although at station L1 it continued to 7 mm and at station L3 to 9 mm displacement.

Compared with the horizontal displacements, the vertical displacements for the left tunnel upper excavation after 8 days were found to be much more consistent (Fig. 9). Similar observations were obtained for the right tunnel upper excavation. Differential displacement profiles for the left tunnel upper excavation are given in Fig. 10 and 11. As the right tunnel was constructed after completion of the left tunnel, not only horizontal displacements but also vertical displacements were observed to be 2–3 times greater than the left tunnel observations. This indicates that the left tunnel construction increases the convergences. This could be because of the small pillar width left between the tunnels which created a larger plastic region around the left tunnel.

The vertical and horizontal displacements around the twin tunnels are given in Figs. 12 and 13. Large vertical displacements were predicted at the bottom of the tunnels (Fig. 12) which suggests that the excavation sequences adopted for tunnel construction were not appropriate. Approximately 120 mm heave at the tunnel invert was predicted. However, there are no field measurements available to verify the FEM prediction for the bottom part of the tunnels. As in many

Fig. 7 Construction sequences adopted in the FE analysis

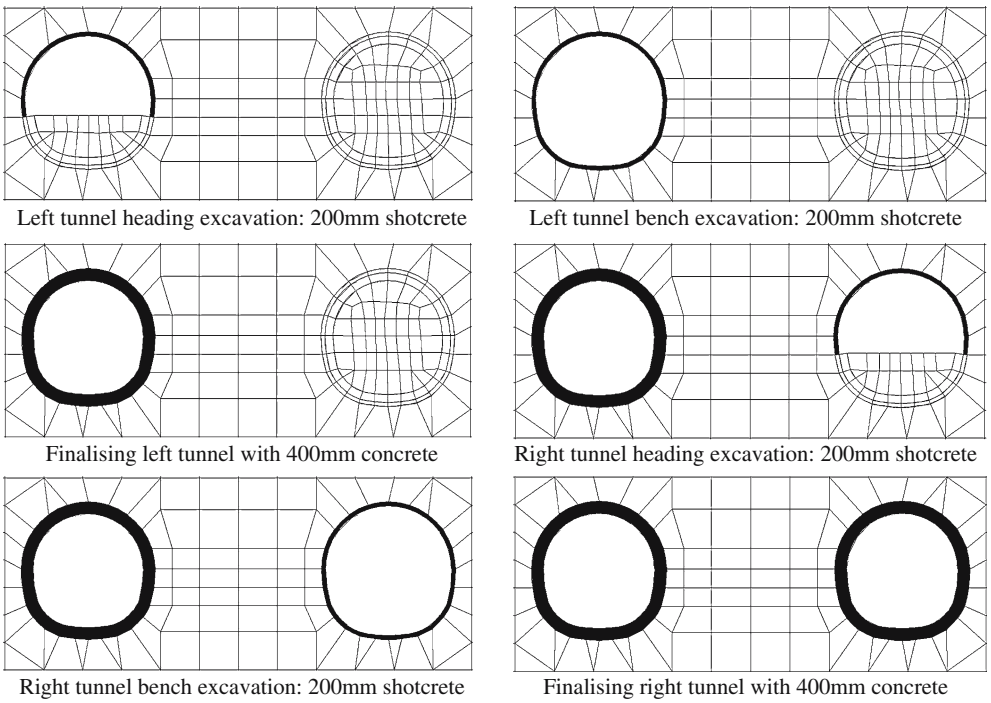

Table 4 Comparison of tunnel convergence for left tunnel

Measurement points at the left tunnel (upper part excavation)	Predictions by FEM (in mm)		Observations (in mm)	
	Vertical	Horizontal	Vertical	Horizontal
L1 at crown	3.4	0.2	3	7
L2 at left sidewall	2.6	2.8	5	6
L3 at right sidewall	2.9	2.4	2	9
Measurement points at the left tunnel (lower part excavation)	Predictions by FEM (in mm)		Observations (in mm)	
	Vertical	Horizontal	Vertical	Horizontal
L1 at crown	3.5	0.2	1	0
L2 at left sidewall	3.6	0.1	2	1
L3 at right sidewall	3.5	0.1	4	7
Measurement points at the right tunnel (upper part excavation)	Predictions by FEM (in mm)		Observations (in mm)	
	Vertical	Horizontal	Vertical	Horizontal
L1 at crown	19.7	1	18	17
L2 at left sidewall	17.8	5.7	16	13
L3 at right sidewall	21.2	2.3	12	11

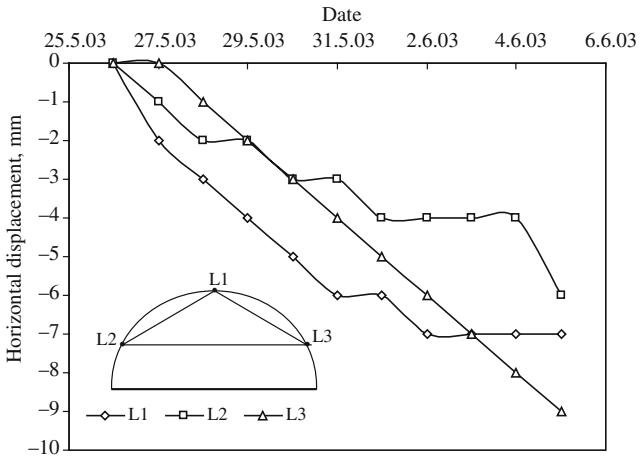

Fig. 8 Observed horizontal displacement for the upper part of the left tunnel

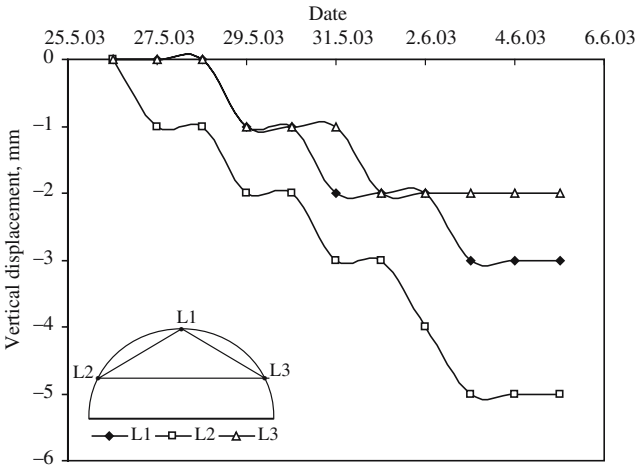

Fig. 9 Observed vertical displacement for the upper part of the left tunnel

cases heave at the tunnel invert causes serious instability problems, field measurements at the bottom part of the tunnel should always be carried out to detect such movements. Horizontal displacements were also concentrated at the sidewalls and bottom part of the tunnels as shown in Fig. 13.

Conclusions

The twin tunnel construction in Ankara Clay was analysed and the geotechnical parameters of the site and convergence profiles monitored during the tunnelling process are presented. The geotechnical properties of the

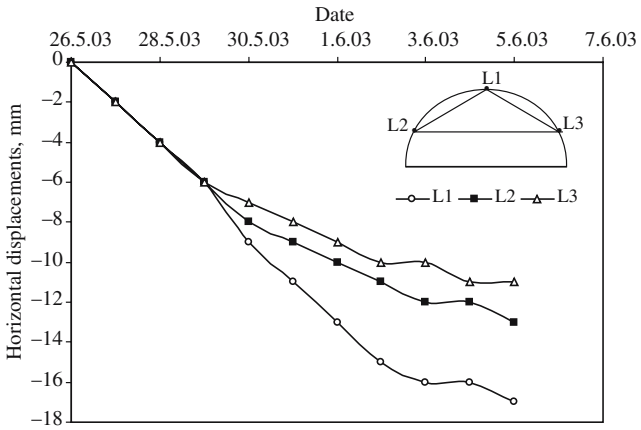

Fig. 10 Measured horizontal displacement on the upper part of the right tunnel

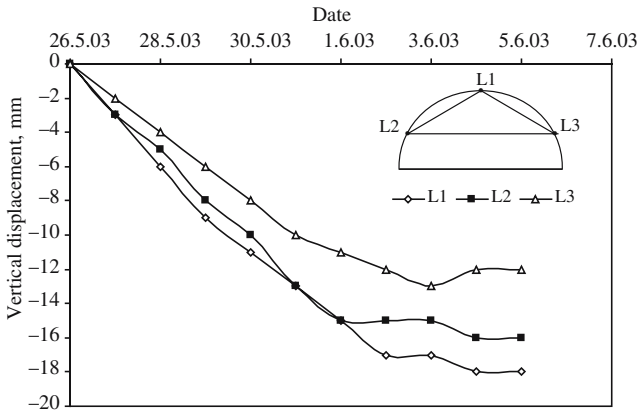

Fig. 11 Measured vertical displacement on the upper part of the right tunnel

construction site were evaluated and parameters for the Modified Cam Clay soil plasticity model were derived from oedometer test results as input data to the FEM analysis.

The results from the numerical analysis show that vertical displacements on the tunnel walls are in agreement with the observations but the horizontal displacements were found to deviate from the actual measurements. However, as the convergence measurements were carried out by topographical methods, the observed convergence could be erroneous. It is therefore considered that a more reliable technique should be used to measure convergence in soft ground.

The right tunnel was constructed after completion of the left tunnel and not only the horizontal displacements but also the vertical displacements were observed to be 2–3 times more than in the left tunnel. It is considered that the earlier left tunnel construction

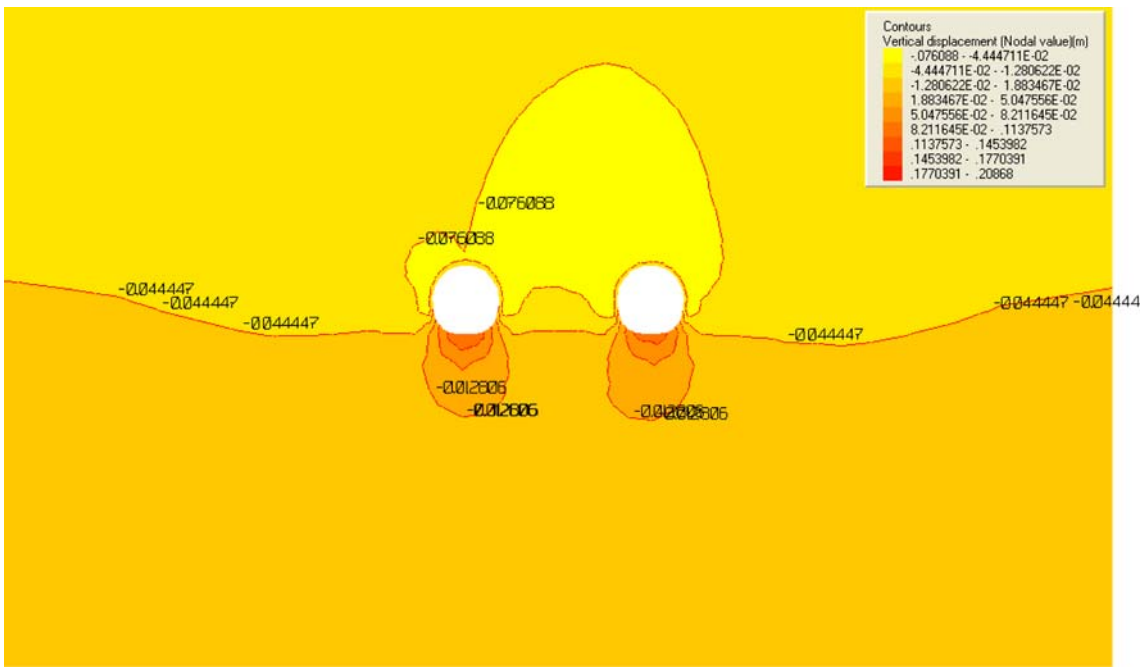

Fig. 12 Vertical displacements around the twin tunnels

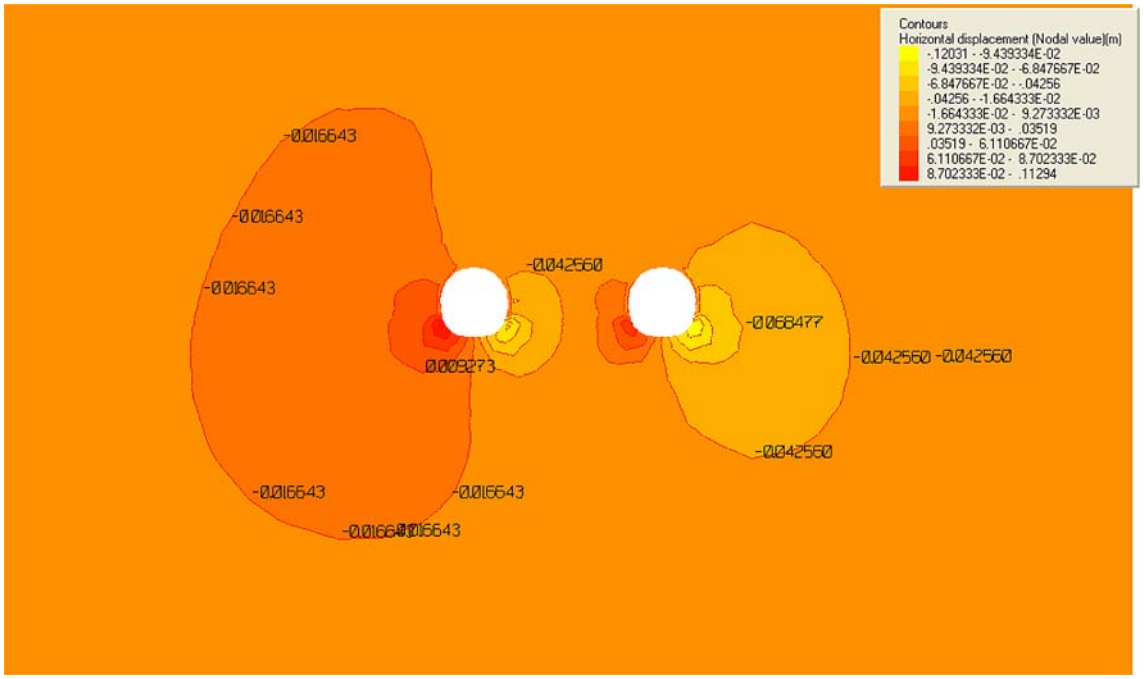

Fig. 13 Horizontal displacements around the twin tunnels

caused/increased in the convergence. This could be due to the small pillar width left between the tunnels which created a larger plastic region around the left tunnel.

Acknowledgments The authors wish to express their deep gratitude to Mr Turker Onur (Geological Engineer) from Yuksel Project International and Mr Fatih Karacan (Geophysical Engineer) from Transportation Rail System of the General Directorate of the EGO for their help during this work.

References

Erguler ZA, Ulusay R (2003) A simple test and predictive models for assessing swell potential of Ankara (Turkey) Clay. Eng Geol 67:331–352

Erol O (1973) Ankara sehri cevresinin jeomorfolojik ana birimleri. AUDTCF Yayınları 240:29, in Turkish

Karakus M, Fowell RJ (2003) Effects of different tunnel face advance excavation on the settlement by FEM. Tunnelling Undergr Space Technol 18(5):513–523

Karakus M, Fowell RJ (2005) Back analysis for the tunnelling induced ground movements and stress redistribution. Tunnelling Undergr Space Technol 20(6):514–524

Kontogianni VA, Stiros SC (2002) Predictions and observations of convergence in shallow tunnels: case histories in Greece. Eng Geol 63:333–345

Kovari K, Amstad C (1993) Decision making in tunnelling based on field measurements. In: Hudson JA (ed) Comprehensive rock engineering, vol. 4. Pergamon, Oxford, pp 571–606

Ordemir I, Alyanak I, Birand AA (1965) Report on Ankara Clay. METU Publication No. 12, Ankara, Turkey

Ordemir C, Soydemir C, Birand AA (1977) Swelling problems of Ankara clays. In: Proceedings of the 9th international conference on soil mechanics and foundation engineering, vol. 1, Tokyo, Japan pp 243–247

Ozsan A, Basarir H (2003) Support capacity estimation of a diversion tunnel in weak rock. Eng Geol 68(3–4):319–331

Ozsan A, Karpuz C (2001) Preliminary support design for Ankara subway extension tunnel. Eng Geol 59:161–172

Roscoe KH, Burland JB (1968) On the generalized stress–strain behaviour of 'wet' clay. In: Engineering plasticity conference, Cambridge pp 535–607

Wood DM (1990) Soil behaviour and critical state soil mechanics. Cambridge University Press, Cambridge pp 113–138